CGMS-XXXI JMA-WP-08
Prepared by JMA
Agenda Item:II/2
Discussed in WG-II

Intercalibration between GMS-5 and GOES-9

The geostationary satellite, GMS-5, was replaced by GOES-9 on 22 May 2003. This working paper reports the result of comparison between imagers aboard the two satellites.

Intercalibration between GMS-5 and GOES-9

Meteorological Satellite Center / Japan Meteorological Agency

Abstract

This study investigates intercalibration between GOES-9 Imager and GMS-5 VISSR infrared channels. For this purpose, GOES-9 and GMS-5 observed and simulated brightness temperatures are used. The observed brightness temperatures are obtained from images observed just before the switchover from GMS-5 to GOES-9; the simulated brightness temperatures are computed by MODTRAN 3.7. In the comparison of the horizontal images, a difference between GOES-9 and GMS-5 is recognized as expected from their spectral response functions and each radiative path. Further, as the result of the statistical comparison of observed brightness temperatures with the same radiative path length from the satellites within the cloud-free ocean area, discrepancies inconsistency with simulations are detected. The averages of the discrepancies between GOES-9 and GMS-5 with respect to residuals of the observed from simulated brightness temperatures are 0.70 K, 0.28 K and 2.4 K for the infrared window channel 1 (IR1), the infrared window channel 2 (IR2) and the water vapor channel (WV) respectively. Potential sources of the differences are inaccurate calibration, the unveiled degradation of the sensors and the satellites, systematic error in the simulated brightness temperatures, etc. In order to identify the source, further research is necessary. Despite the sources are unconfirmed, the result of this study may be of help to revise the algorithms of GOES-9 applications. For instance, linear relationship is found between GOES-9 and GMS-5 with respect to difference between the IR1 and IR2 brightness temperatures.

Introduction

The Geostationary Meteorological Satellite 5 (GMS-5) was launched on 18 March 1995 carrying the Visible and Infrared Spin Scan Radiometer (VISSR) to provide cloud and water vapor images over the west Pacific region. Its observation had lasted for 8 years exceeding the designed lifetime of 5 years. Due to the shortage of fuel for satellite orbital control and the degradation of the mirror controller in VISSR, the Geostationary Operational Environmental Satellite 9 (GOES-9) started its operational observation over the west Pacific region on 22 May 2003 substituting for GMS-5. GOES-9 also carries an imager, called GOES-9 Imager, providing cloud and water vapor images successively.

Figure 1 shows the examples of infrared images observed by (a) GOES-9 Imager and (b) GMS-5 VISSR at a time. The two images provide the similar information of cloud and weather systems except for 15-longitude-degree difference in the observed region. The information is precious for not only weather and climate watch, but also generating physical parameters such as atmospheric wind vectors, aerosol, volcanic ash and sea ice, etc. Therefore, it is important to survey difference in the images between GOES-9 Imager and GMS-5 VISSR in order to maintain the accuracy of the products. This paper reports the results of comparisons between images simultaneously observed just before the switchover from GMS-5 to GOES-9. In GOES-9 images of GVAR data, some noise is contained as shown in Figure 2. The noise is noted in the end of this paper additionally.

Comparison of Specifications

GMS-5 flies in a geosynchronous orbit at 140 E.VISSR aboard GMS-5 has four channels; two channels are in the infrared window region (IR1 and IR2), the other two channels are in the infrared water vapor region (WV) and the visible region (VIS) respectively. Table 1 shows the spectral bands and the spatial resolutions of these channels. The details of calibration for GMS-5 VISSR are found in MSC, 1997, Tokuno et al, 1997 and Kurihara et al, 2000.

GOES-9 has been placed in a geosynchronous orbit at 155 E since 25 April 2003. Its operational observation at the longitude started on 22 May. Imager aboard GOES-9 has five channels; four of them have similar spectral bands to VISSR, and one additional channel is in the short wave infrared window region (SWIR). The spectral bands and the resolutions of these channels are shown in Table 1 as well as IR1. The details of calibration for GOES-9 Imager are found in ‘GOES Data Book’ by NASA, 2001 and the web pages of NASA and

NESDIS on the Internet. To avoid confusion caused by resemblance between the sensor name GOES “Imager” and the sensor’s category name “imager”, simply satellite name is used to denote onboard sensor hereafter.

Figure 3 shows the spectral response functions of the infrared channels of (a) GOES-9 and (b) GMS-5 as a function of wavenumber. IR2 is located in a smaller wavenumber region than IR1 for GOES-9 and GMS-5 respectively. GOES-9 IR1 and GMS-5 IR1 are approximately in the same spectral region with each other, while GOES-9 IR2 is in a smaller wavenumber region than GMS-5 IR2. Water vapor continuum is the major source of absorption for IR1 and IR2. The absorption becomes larger, as wavenumber is smaller. Hence, IR2 is more affected by the absorption than IR1, and GOES-9 IR2 is more affected than GMS-5 IR2. The WV channels of GOES-9 and GMS-5 are in the spectral region of strong absorption by water vapor transition. Since GOES-9 WV is in a larger wavenumber region than GMS-5 WV, GOES-9 WV is more affected by the absorption than GMS-5 WV. The large absorption, consequently less transparent, makes brightness temperature low. Therefore, the IR2 brightness temperatures of GOES-9 and GMS-5 are expected to be lower than the IR1 brightness temperatures of GOES-9 and GMS-5 respectively. Similarly, the brightness temperatures of GOES-9 IR2 and WV are lower than those of GMS-5 IR2 and WV respectively.

Figure 4 shows the spectral response functions of GOES-9 VIS (thin lines) and GMS-5 VIS (thick line) as a function of wavelength. The spectral band of GOES-9 VIS is narrower than that of GMS-5 VIS. That may affect on some products using the VIS channel, such as volcanic ash and aerosol. However, the VIS channels aren’t compared in this study, since the geosynchronous orbital difference between GOES-9 and GMS-5 makes the comparison difficult. A polar-orbiting satellite is necessary for the intercalibration of VIS.

The difference in the geosynchronous orbits makes a difference in radiative path through the atmosphere from the earth surface to the two satellites. Assuming atmosphere is plain parallel and homogeneous at each observing point, the difference in radiative path is equivalent to that in the path length. A longer radiative path makes atmospheric absorption and scattering effects larger. Figure 5 shows secant of satellite zenith angles of GOES-9 (a) and GMS-5 (b), which are approximately proportional to the path lengths. Fig. 5 (c) shows the difference between the figure (a) and (b). The lengths from the longitude line at 147.5 E to the two satellites are equal. A length from the surface to GOES-9 is longer than that to GMS-5 on the west side of 147.5 E, and vice versa on the east side.

Comparison of Images

Figure 6 (a) and (b) show the images of IR1 brightness temperatures of 06 UTC 19 May 2003 observed by GOES-9 and GMS-5 respectively. The figure (c) shows the differences computed by subtracting the temperatures of the figure (b) from those of the figure (a). The figure (d) shows the same as the figure (c) but for brightness temperatures simulated by the Moderate Resolution Model for LOWTRAN 7 (MODTRAN 3.7) (Berk et al, 1989). In the simulation, any atmospheric scattering is neglected.

Atmospheric absorption is estimated by using the three-dimensional grid data of atmospheric fields forecasted by the global numerical weather prediction model of the Japan Meteorological Agency. The data is interpolated to 1.25-degree grids with 16 vertical levels up to 10 hPa. The simulation is performed only over the ocean, while surface emissivity is assumed to be 0.98 in invariable.

It is impossible to recognized distinct difference between the GOES-9 image in the figure (a) and the GMS-5 one in the figure (b). However, the figure (c) indicates that the difference between the images has a zonal trend. The simulated difference shown in figure (d) also represents the same trend. The trend is caused in association with the difference in radiative path lengths to the two satellites. Regarding the clear sky and low cloud areas colored in red and orange in the figure (a) and (b), the zonal trends seen in the figure (c) and (d) are approximately the same with each other. The zonal trend in the figure (c) is enhanced over the thin cloud and wet atmosphere areas drawn in light blue and green in the figure (a) and (b). Regarding the thick cloud areas colored in dark blue in the figure (a) and (b), the differences between the satellites in the figure (c) are small and drawn in green, particularly over SPCZ and ITCZ. The differences are negative over the Bay of Bengal and the South China Sea, even though dark blue points are observed there in the figure (a) and (b). The feature is inconsistent to being recognized over SPCZ and ITCZ. The reason is that only upper thin cloud covers over the Bay of Bengal and the South China Sea at the time.

Figure 7 shows the same comparisons as Fig. 6, but for IR2 images. Similar to IR1, distinct difference cannot be recognized in observed images between the figure (a) and (b). A zonal trend similar to IR1 is seen in the figure (c) and (d). Comparing Fig. 6 (c) and 7 (c) over the clear sky area, the IR2 brightness temperature residuals of GOES-9 from GMS-5 are lower than the IR1 residuals. The similar feature is recognized in the simulated images between Fig. 6 (d) and 7 (d). In terms of the relation to the cloudy areas, the same discussion can be conducted as IR1; the large zonal trend over the thin cloud, the small differences over the thick cloud.

Figure 8 shows the same comparisons as Fig. 6, but for differences in brightness temperatures between the split window channels, $\delta T_{SP} = T_{IR1} - T_{IR2}$. The positive δT_{SP} of GOES-9 dominate over the Tropics as shown in the figure (a) due to the difference in the water vapor absorption between IR1 and IR2. δT_{SP} decrease in the mid-latitude, where moisture in the atmosphere is less than the Tropics. Neutral δT_{SP} are recognized corresponding to the cloud. GMS-5 image in the figure (b) shows the similar features to GOES-9. However, δT_{SP} of GMS-5 are smaller than those of GOES-9, since the difference in the spectral response functions between GMS-5 IR1 and IR2 is small. The figure (c) and (d) don't show clear zonal trend. This denotes that the differences in δT_{SP} between GOES-9 and GMS-5 are zero or negatively correlated with path lengths.

Figure 9 shows the same comparisons as Fig. 6, but for WV images. The brightness temperatures of GOES-9 in the figure (a) are lower than those of GMS-5 in the figure (b), since GOES-9 WV is less transparent than GMS-5 WV. The observed differences between GOES-9 and GMS-5 in the figure (c) are less than the simulated differences in the figure (d). This inconsistency will be discussed in the next section.

Comparison of Statistics

The differences between the image data of GOES-9 and GMS-5 shown in Fig. 6 to 9 are originated in the characteristics of the sensors and the radiative paths. In order to survey the difference associated with the sensors, the brightness temperatures are compared statistically. The method of the comparison is referred to Gunshor et al (2001). The region for the comparison is from 140 E to 155 E and from 45 S to 45 N, where radiative path lengths from the earth surface to the two satellites are approximately the same. The observational times of the data used in this study are at 00, 06, 12 and 18 UTC on 19 May 2003. In order to match up the observations between GOES-9 and GMS-5, the brightness temperatures are averaged in 0.25 latitude and longitude degree boxes. The averaged temperatures, whose box domains are entirely over the ocean and the cloud free, are only applied to the statistical computation. For the elimination of the cloudy data, the technique of cloud detection used in the SST retrieval (Yasuda and Shirakawa, 1999) is applied. The brightness temperatures simulated by MODTRAN 3.7 are also evaluated. Matching up the brightness temperatures between the observations and the simulations of GOES-9 and GMS-5 respectively, 68 sets of the brightness temperatures are obtained.

Figure 10 shows the comparisons of the IR1 brightness temperatures. The figure (a) and (b) show comparisons between the observed and simulated temperatures of GOES-9 and GMS-5

respectively. The figure (c) and (d) show comparisons between GOES-9 and GMS-5 of the observed and simulated temperatures respectively. Points in the figure (c) and (d) are located along with the diagonal lines, while the points are spread across the lines in the figure (a) and (b). This suggests that the diffusion of the points is generated by systematic error in the simulated brightness temperatures. The diffusive error is mainly originated from inaccuracy in the water vapor and sea surface temperature fields computed by the numerical weather prediction system and incorrectness in the water vapor absorption estimated by MODTRAN.

The observed brightness temperatures of GOES-9 are higher than those of GMS-5 as recognized in the figure (c). On the other hand, the simulated brightness temperatures of GOES-9 are less biased to those of GMS-5 in the figure (d), as expected by the similarity of the spectral bands between GOES-9 IR1 and GMS-5 IR1. Therefore, the difference in the spectral response functions cannot explain the discrepancy recognized in the figure (c). The figure (e) shows comparison between GOES-9 and GMS-5 with respect to the residuals of the observed brightness temperatures from the simulated temperatures. The figure (f) shows comparison between observation and simulation with respect to the residuals of the GOES-9 brightness temperatures from the GMS-5 temperatures. The departures of the points from the diagonal lines in the figure (e) and (f) represent discrepancies in the observations between GOES-9 and GMS-5 unpredicted by the simulation. The average of the unpredictable discrepancies,

$$\overline{\delta T}^{\mathrm{GOES9-GMS5}}_{\mathrm{IR1,obs-cal}} = < (T^{\mathrm{GOES9}}_{\mathrm{IR1,obs}} - T^{\mathrm{GOES9}}_{\mathrm{IR1,cal}}) - (T^{\mathrm{GMS5}}_{\mathrm{IR1,obs}} - T^{\mathrm{GMS5}}_{\mathrm{IR1,cal}}) >$$

is +0.70 K.

Figure 11 shows the same comparisons as Fig. 10, but for IR2 brightness temperatures. Diffusion similar to Fig. 10 (a) and (b) can be recognized in Fig. 11 (a) and (b) respectively. The diffusion in Fig. 11 (a) is slightly larger than that in the figure (b), since the water vapor absorption of GOES-9 IR2 is larger than that of GMS-5 IR2 and increases its estimation error. As shown in the figure (c) and (d), the brightness temperatures of GOES-9 are smaller than those of GMS-5, that is expected in Section 2. As well as IR1, there are the discrepancies in the IR2 observed brightness temperatures between GOES-9 and GMS-5 unpredicted by the simulation. The average of the unpredictable discrepancies, $\overline{\delta T}^{\mathrm{GOES9-GMS5}}_{\mathrm{IR2,obs-cal}}$, is +0.28 K.

Figure 12 shows the same comparisons as Fig. 10, but for the brightness temperature differences of IR1 from IR2, $\delta T_{\mathrm{SP}} = T_{\mathrm{IR1}} - T_{\mathrm{IR2}}$. As shown in Fig. 12 (c), the observed δT_{SP} of

GOES-9 are larger than those of GMS-5. The fact is expected from the discussion about the spectral response functions in Section 2 and simulated in the figure (d). However, inconsistency is recognized between the figure (c) and (d). The average of the discrepancies in the observations between GOES-9 and GMS-5 unpredicted by the simulation, $\overline{\delta T}^{\mathrm{GOES9-GMS5}}_{\mathrm{SP,obs-cal}}$, is +0.42 K. As seen in the figure (c) and (d), δT_{SP} of GOES-9 and GMS-5 have linear relationship with each other given by

$$\delta T^{\mathrm{GOES9}}_{\mathrm{SP,obs}} = 2.09\delta T^{\mathrm{GMS5}}_{\mathrm{SP,obs}} + 0.65 \quad \text{(observation)},$$
$$\delta T^{\mathrm{GOES9}}_{\mathrm{SP,cal}} = 1.77\delta T^{\mathrm{GMS5}}_{\mathrm{SP,cal}} + 0.28 \quad \text{(calculation)},$$

respectively. These equations may be of help to transform a GMS-5 product to a GOES-9 one, which uses δT_{SP} in its retrieval.

Figure 13 shows the same comparisons as Fig. 10, but for WV brightness temperatures. The points in the Fig. 13 (a) and (b) are spread wider than those seen in Fig. 6 for IR1 and Fig. 7 for IR2. Erroneousness in the estimation of the large water vapor absorption is enhanced. Many points in the figure (b) are positioned around the diagonal line, while the plots are above the diagonal line in the figure (a). However, the fact does not denote that the GMS-5 observations are more accurate than the GOES-9 observations, because the brightness temperature simulation could have the same systematical error as that the GMS-5 observations have. The figure (c) and (d) shows that the brightness temperatures of GOES-9 are smaller than those of GMS-5, since the water vapor absorption for GOES-9 is larger than that for GMS-5. Averaged difference in the observed brightness temperatures of GOES-9 from GMS-5 is –5.27 K, while averaged difference in the simulated temperatures is –7.60 K. The inconsistencies between the observations and the simulations are obviously recognized in the horizontal images shown in Fig. 9 (c) and (d). As well as IR1 and IR2, there are the discrepancies between the GOES-9 and GMS-5 WV observed brightness temperatures unpredicted by the simulation. The average of the unpredictable discrepancies, $\overline{\delta T}^{\mathrm{GOES9-GMS5}}_{\mathrm{WV,obs-cal}}$, is +2.4 K.

Conclusion

The infrared images simultaneously observed by GOES-9 Imager and GMS-5 VISSR are compared. In addition, simulated images computed by MODTRAN 3.7 are compared. The

differences between GOES-9 and GMS-5 are observed as expected from their spectral response functions and each radiative path. The distinct inconsistencies are also recognized between the observed and simulated WV images.

Statistical comparison is also studied. Brightness temperatures from the images are compared over the cloud free ocean and the same path lengths. The differences between the GOES-9 and GMS-5 observed brightness temperatures are recognized. The differences are not equivalent to those in the simulated brightness temperatures for not only WV but also IR1 and IR2. The averages of the discrepancies in the observed brightness temperatures between GOES-9 and GMS-5 unpredicted by the simulation, $\overline{\delta T}^{\mathrm{GOES9-GMS5}}_{\mathrm{obs-cal}}$, are +0.70 K, +0.28 K and +2.4 Kfor IR1, IR2 and WV respectively.

The potential sources of the discrepancies are inaccurate calibration, unveiled degradation in the sensors and satellites, the retrieval error of the spectral response functions, and systematic error in the brightness temperatures simulated by MODTRAN 3.7 and atmospheric fields computed by the numerical weather prediction model, etc. In order to identify the sources, further research is necessary.

Despite the sources are unconfirmed, the discussion in Section 3 and 4 may be of help to revise the algorithms of GOES-9 applications. For instance, linear relationship is found between GOES-9 and GMS-5 with respect to difference between IR1 and IR2 brightness temperatures.

Notes

Some noise is recognized in GOES-9 images contained in GVAR data generated by NESDIS. Figure 2 (a) shows an enlarged image observed by GOES-9 VIS. Anomalous noise can be recognized. In order to eliminate it, a digital filtering technique, which consists of a band pass filter with an amplitude limitation, is applied at the Meteorological Satellite Center. The details of the noise reduction technique can be found in Kigawa et al, 2002.

Stripe noise associated with scan lines can also be observed in GOES-9 IR1 and IR2 images contained in GVAR data. The noise is only recognized in the range of brightness temperature higher than 293 K, even though temperature should be homogeneous over cloud free ocean. The variation of the noise is approximately 0.5 K for IR2 and 0.2 K for IR1. The noise is negligible to observe weather systems from GOES-9 images. However, it may not be

negligible to retrieve physical quantities. For instance, the influence of the noise is emphasized in difference between IR1 and IR2 brightness temperatures as shown in Fig. 2 (b). The noise may cause the degradation of some products. In order to eliminate the stripe noise, further research is needed as well.

Reference

Berk, A., L.S. Bernstein and D.C. Roberson, 1989: MODTRAN: A Moderate Resolution Model for LOWTRAN 7. GL-TR-89-0122.

Gunshor, M. M., T. J. Schmit and W. P. Menzel, 2001: Intercalibration of geostationary and polarorbiting infrared window and water vapor radiances. Extended Abstracts, Eleventh Conf. on Satellite Meteorology and Oceanography, Madison, Wisconsin, Amer. Meteor. Soc., 438-441.

Kigawa, S. and D. Chesters, 2002: Digital Noise Filter for GOES-9 Visible Channel. Meteorological Satellite Center Technical Note, No. 41, 21-35.

Kurihara, S. and M. Tokuno, 2000: The Status of Calibration of VISSR on board GMS-5. Meteorological Satellite Center Technical Note, No. 38, 53-68. (written in Japanese)

Meteorological Satellite Center, 1997: The GMS User's Guide Third Edition.

NASA, 2001: GOES Data Book.

Tokuno, M., H. Itaya, K. Tsuchiya and S. Kurihara, 1997: Calibration of VISSR Onboard GMS-5. Adv. Space Res., 19, 9, 1297-1306.

Yasuda, Hiroaki and Yoshishige Shirakawa, 1999: Improvement of the Derivation Method of Sea Surface Temperature from GMS-5 Data. Meteorological Satellite Center Technical Note, No. 37, 19-33. (written in Japanese)

NASA: 'GOES Project Science by NASA'.
http://rsd.gsfc.nasa.gov/goes/

NOAA/NESDIS: 'Geostationary Operational Environmental Satellites'.
http://www.oso.noaa.gov/goes/

(a) GOES-9 Imager IR1 (b) GMS-5 VISSR IR1

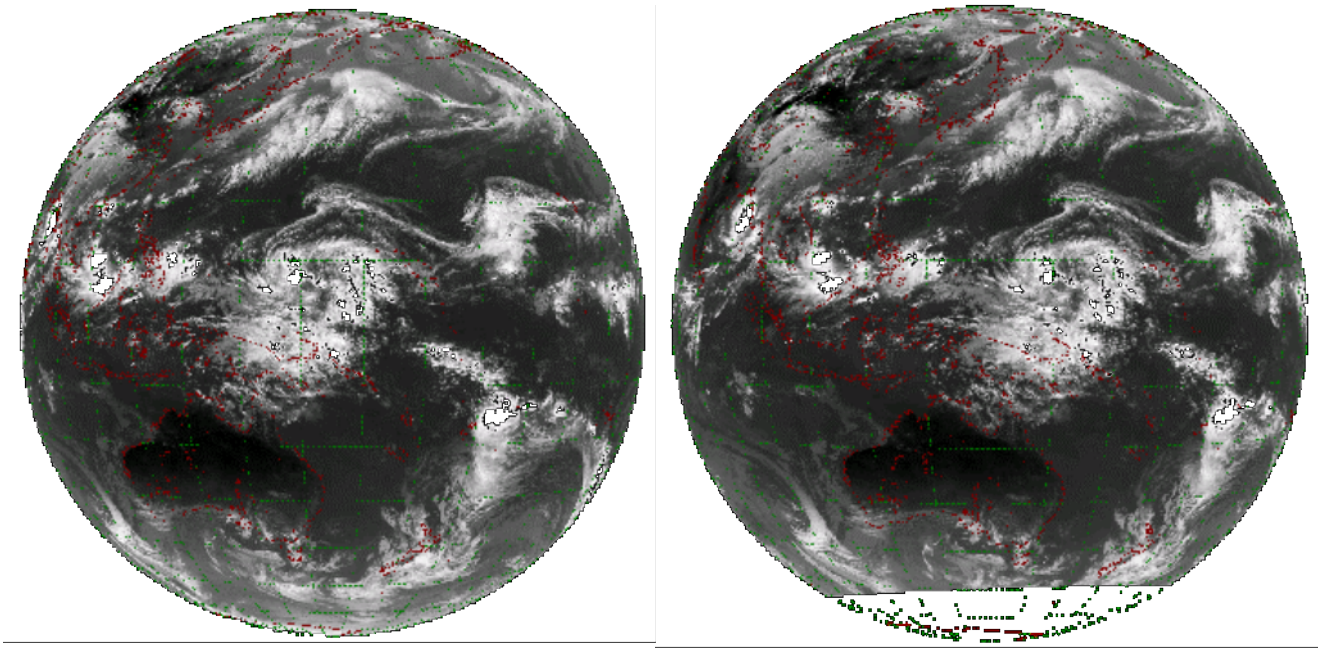

Figure 1: Cloud images observed by the IR1 channels of GOES-9 Imager (a) and GMS-5 VISSR (b) at 06 UTC on 19 May 2003.

(a) GOES-9 Imager VIS (b) GOES-9 Imager IR1 minus IR2

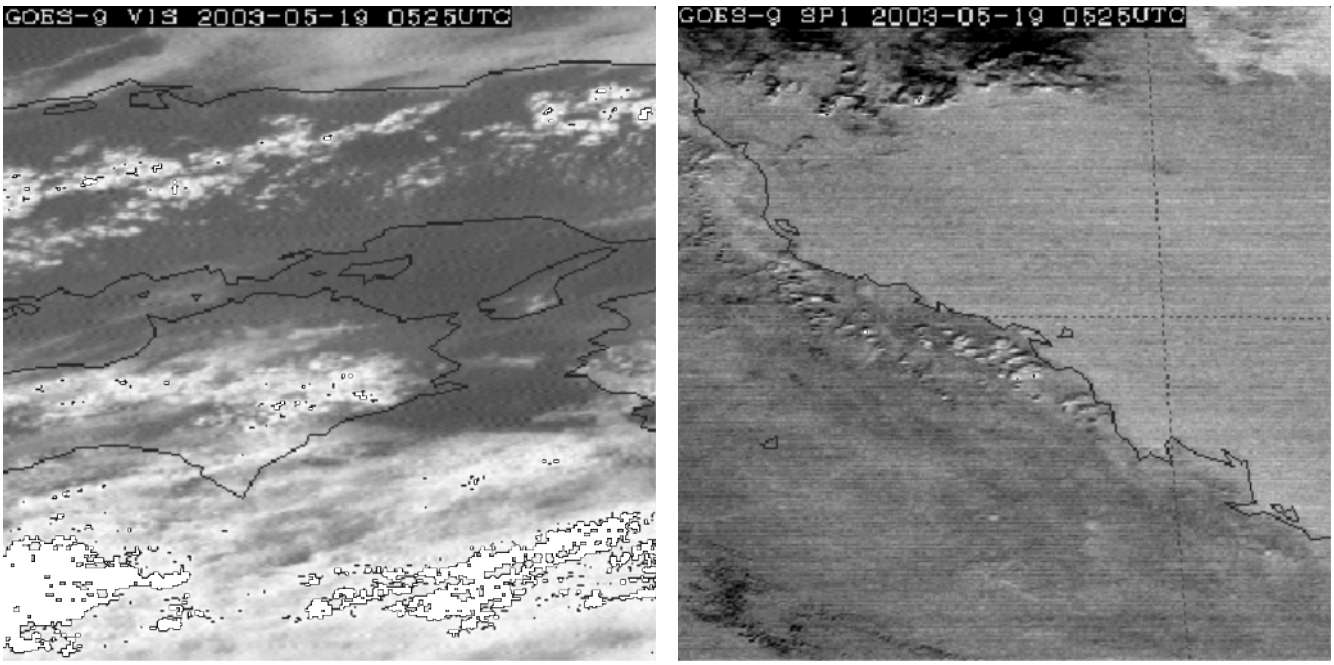

Figure 2: Images observed by GOES-9 Imager of (a) the VIS channel over the western Japan and (b) the difference in the brightness temperatures between GOES-9 IR1 and IR2 over the north east Australia. The observational time is the same as Figure 1.

(a)

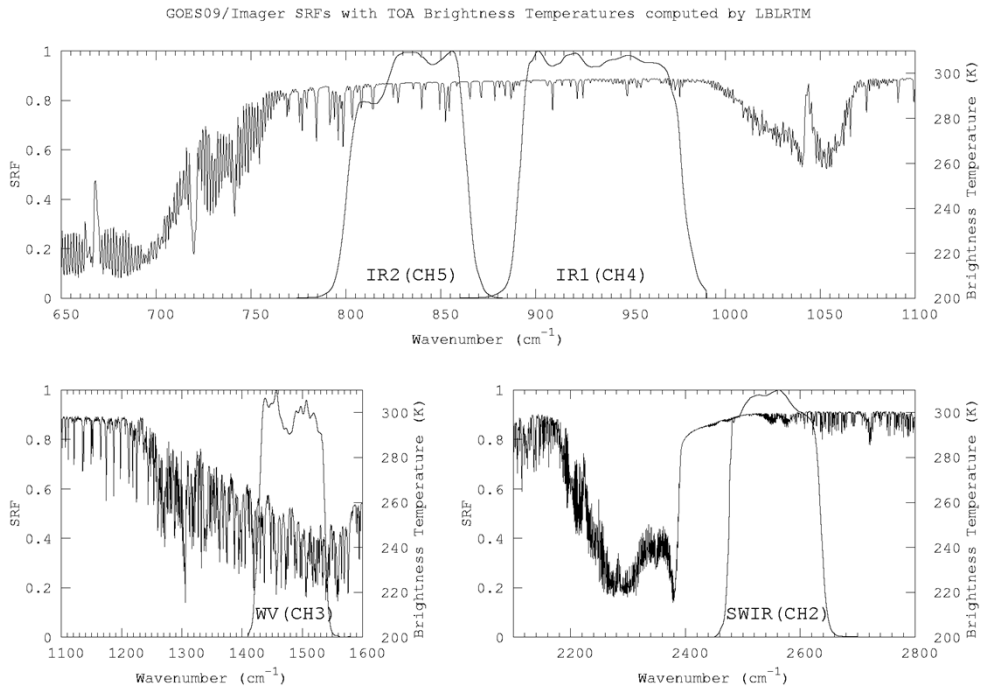

(b)

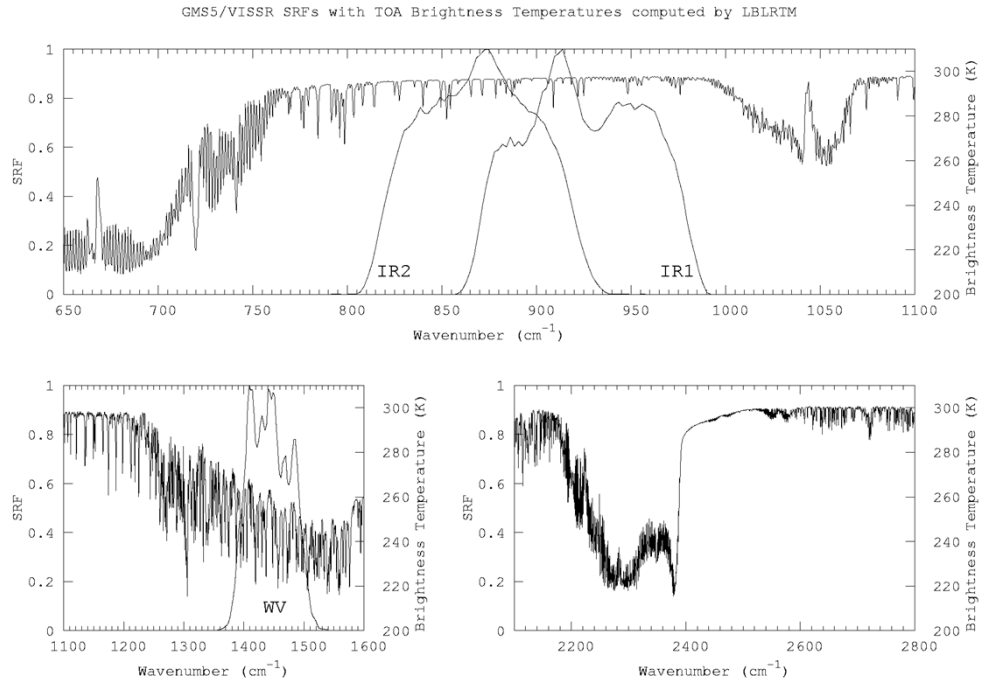

Figure 3: Spectral response functions of the infrared channels of GOES-9 Imager (a) and GMS-5 VISSR (b) as a function of wavenumber. The thin line represents the brightness temperatures of out-going radiances from top of atmosphere computed by LBLRTM using the U.S. standard atmosphere.

Table 1: Comparison of specifications between GOES-9 Imager and GMS-5 VISSR. The resolutions represent footprint sizes near nadir.

Satellite/Sensor	GOES-9/Imager		GMS-5/VISSR	
Geosynchronous position	155 E		140 E	
Channels	Wavelength	(Res.)	Wavelength	(Res.)
VIS (Visible)	0.55 – 0.75	(1km)	0.55 – 0.9	(1.25km)
IR1 (IR Window 1)	10.2 – 11.2	(4km)	10.5 – 11.5	(5km)
IR2 (IR Window 2)	11.5 – 12.5	(4km)	11.5 – 12.5	(5km)
WV (Water Vapor)	6.5 – 7.0	(8km)	6.5 – 7.0	(5km)
SWIR (Short Wave IR)	3.8 – 4.0	(4km)	(NA)	(NA)

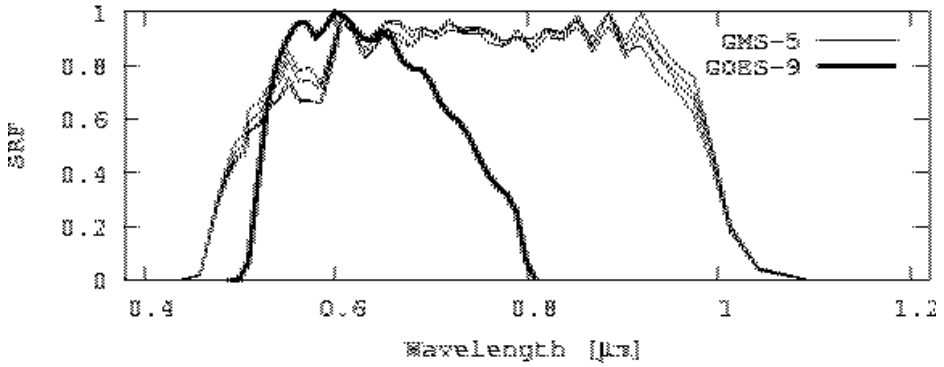

Figure 4: Spectral response functions of the visible channels of GOES-9 Imager (thin lines) and GMS-5 VISSR (thick line).

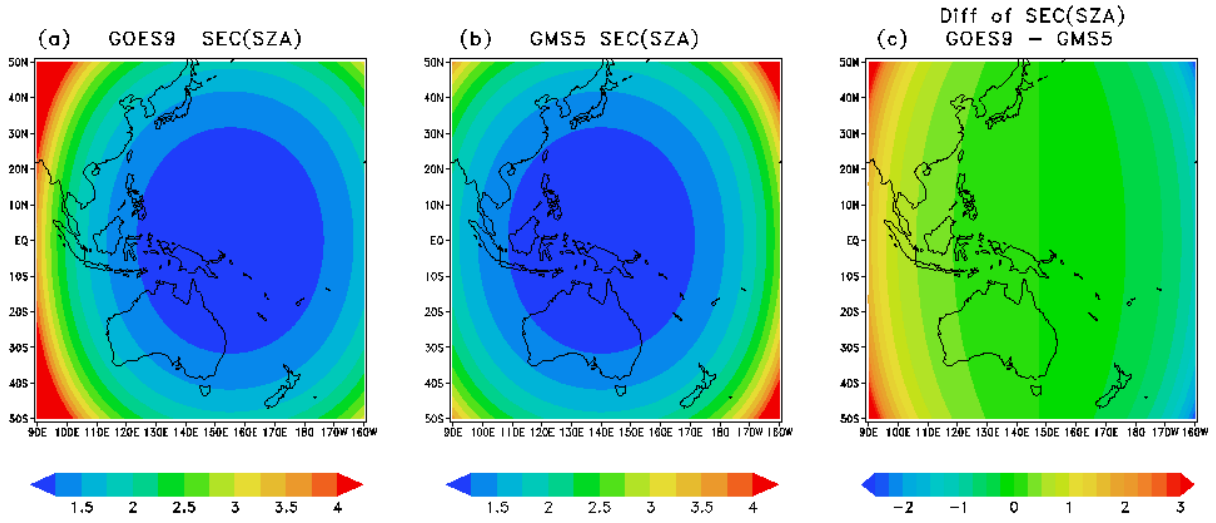

Figure 5: Secant of satellite zenith angles to GOES-9 (a) and GMS-5 (b). The figure (c) shows difference calculated by subtracting the figure (b) from the figure (a).

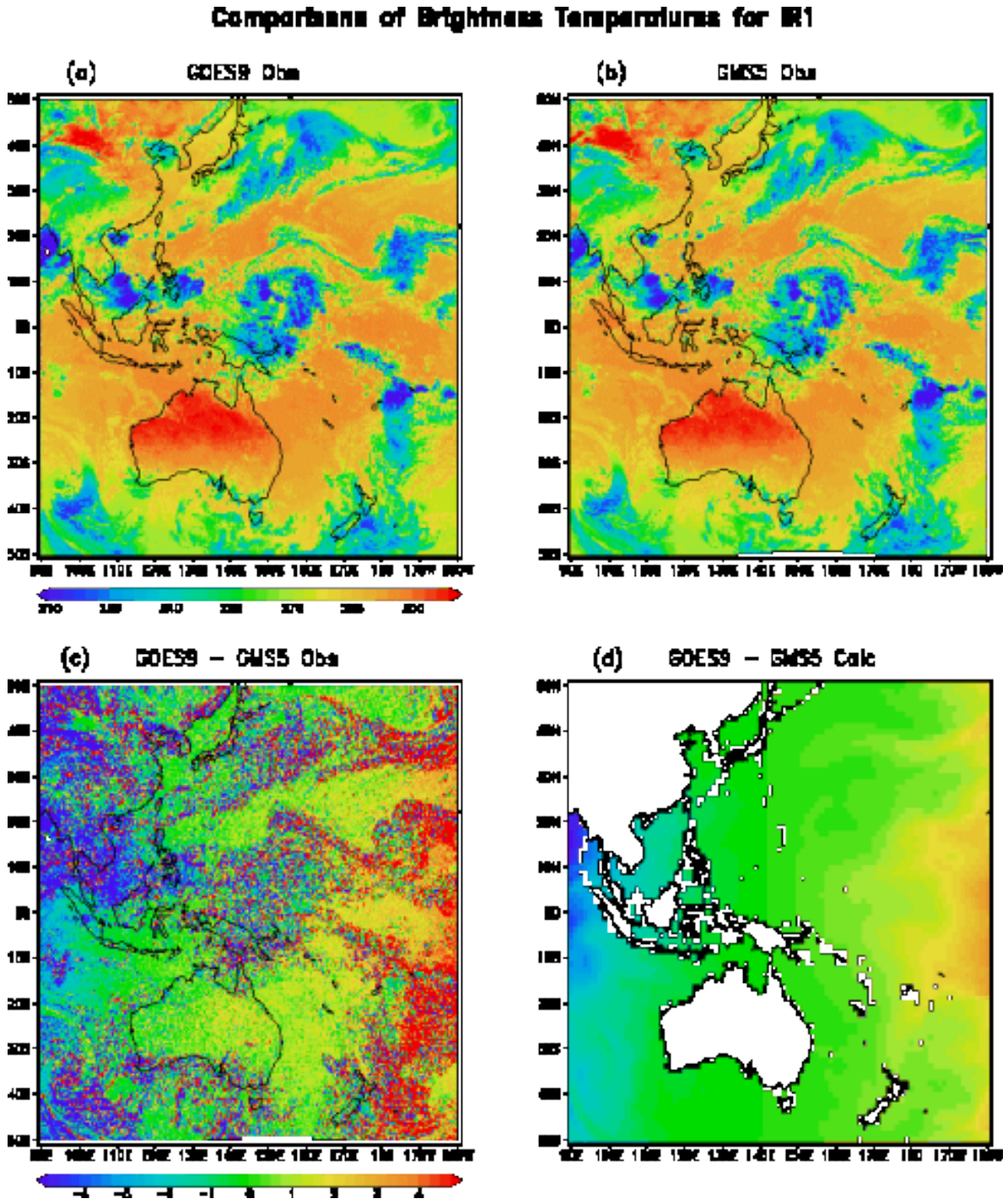

Figure 6: Images of brightness temperatures observed by GOES-9 IR1 (a) and GMS-5 (b). The figure (c) shows the difference in the observed brightness temperatures of GOES-9 from that of GMS-5. The figure (d) shows the same as the figure (c) but for the difference in the simulated brightness temperatures. The simulated temperatures are computed by MODTRAN neglecting atmospheric scattering effect.

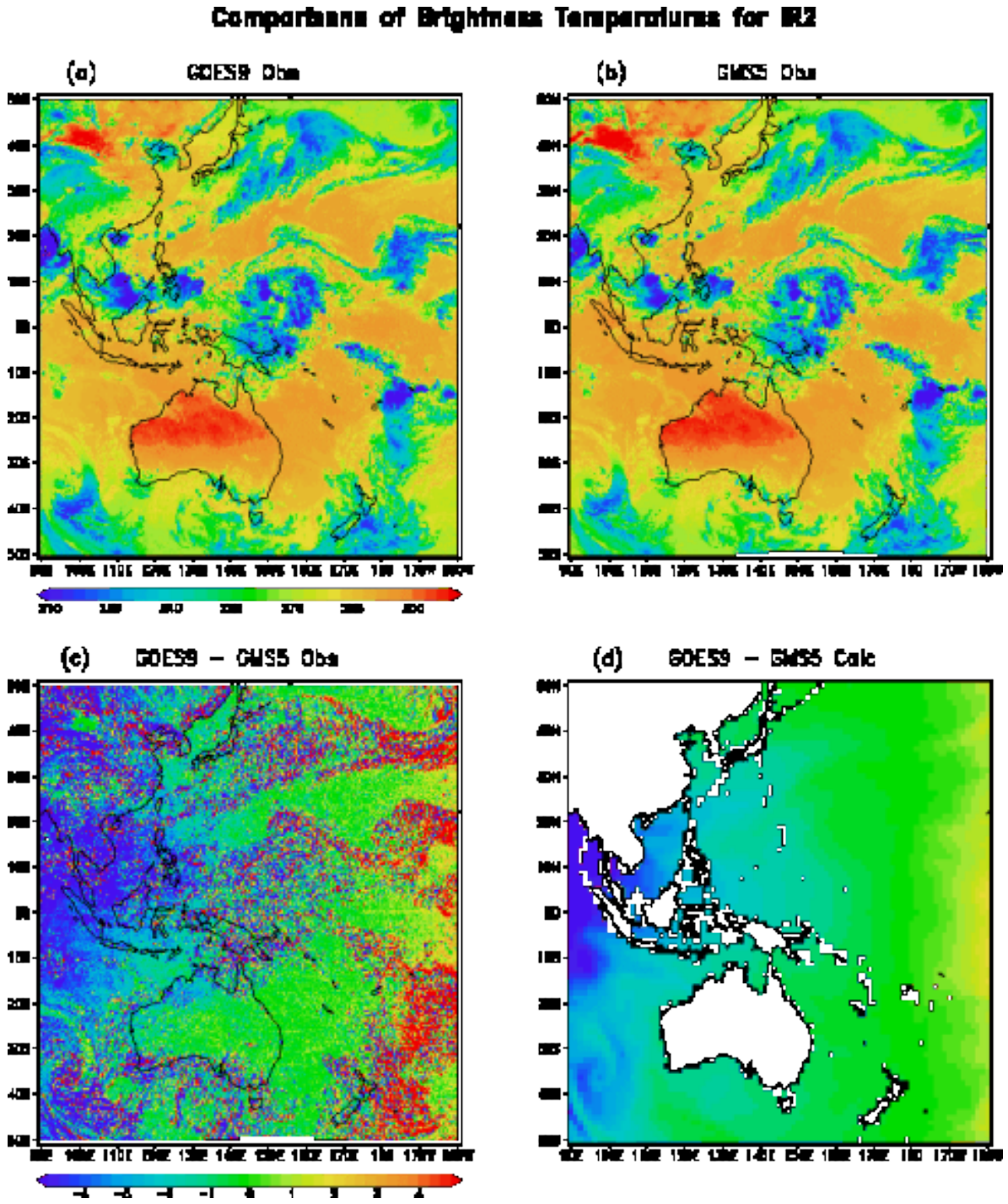

Figure 7: Same as Fig. 6, but the comparisons of IR2 images.

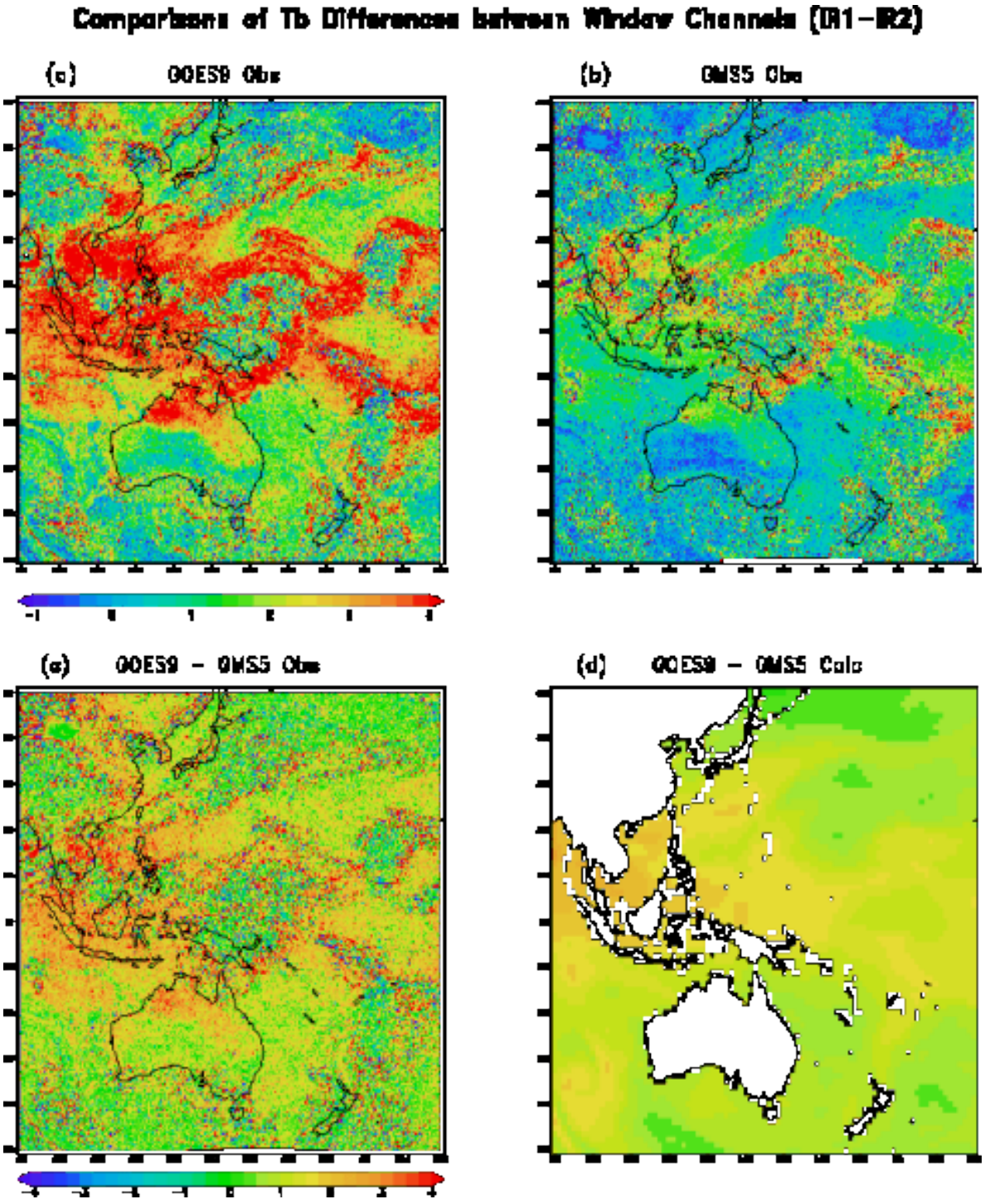

Figure 8: Same as Fig. 6, but the comparisons of differences in the brightness temperatures between the split window channels, $\delta T_{\mathrm{SP}} = T_{\mathrm{IR1}} - T_{\mathrm{IR2}}$.

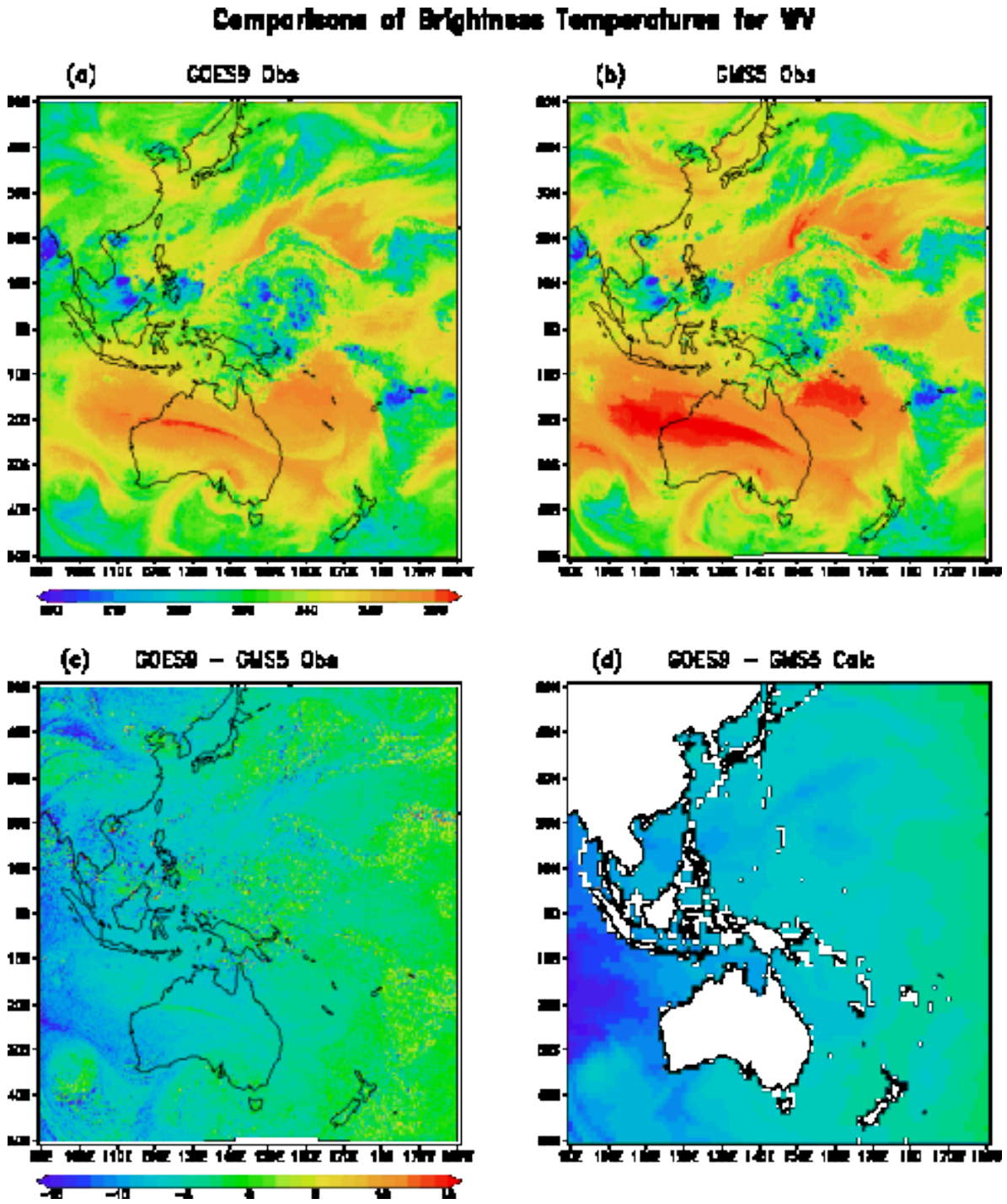

Figure 9: Same as Fig. 6, but the comparisons of WV images.

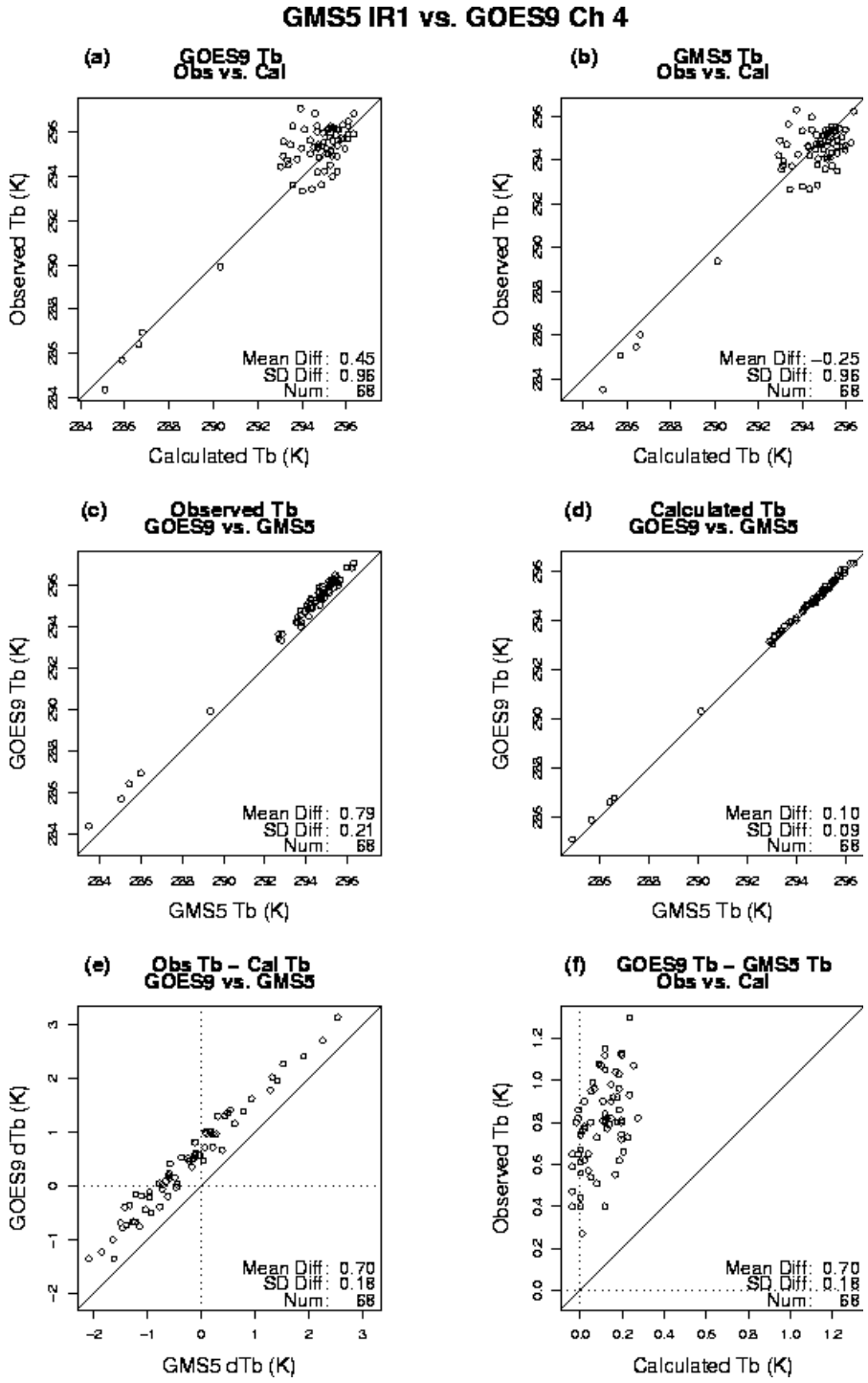

Figure 10: Comparisons of IR1 brightness temperatures; (a) GOES-9 observations versus GOES-9 simulations, (b) GMS-5 observations versus GMS-5 simulations, (c) GOES-9 observations versus GMS-5 observations, (d) GOES-9 simulations versus GMS-5 simulations, (e) observations minus simulations of GOES-9 versus those of GMS-5 and (f) GOES-9 minus GMS-5 of observations versus those of simulations. Mean difference and standard deviation between vertical element and horizontal element are shown as well as the number of samples.

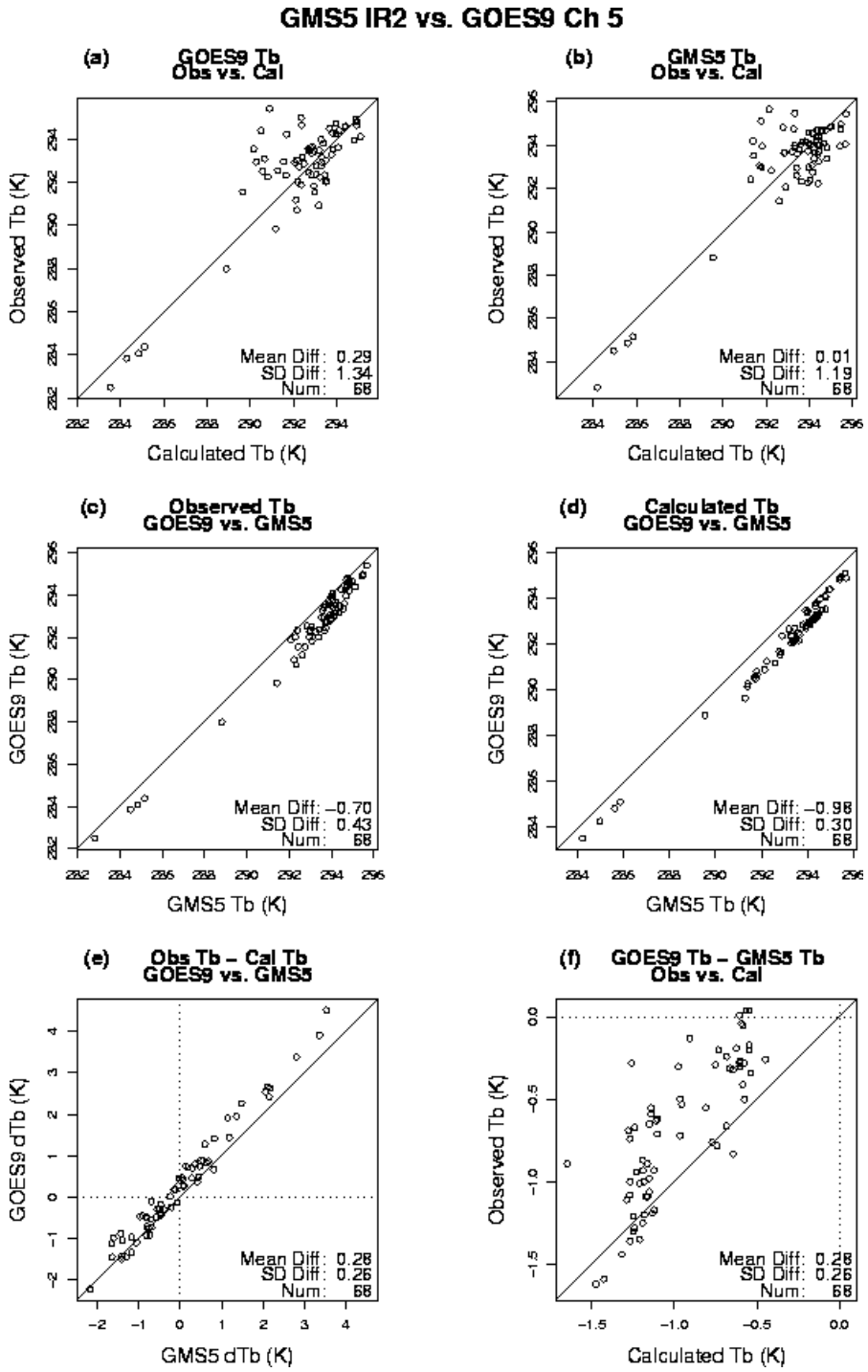

Figure 11: Same as Fig. 10, but the comparisons of IR2 brightness temperatures.

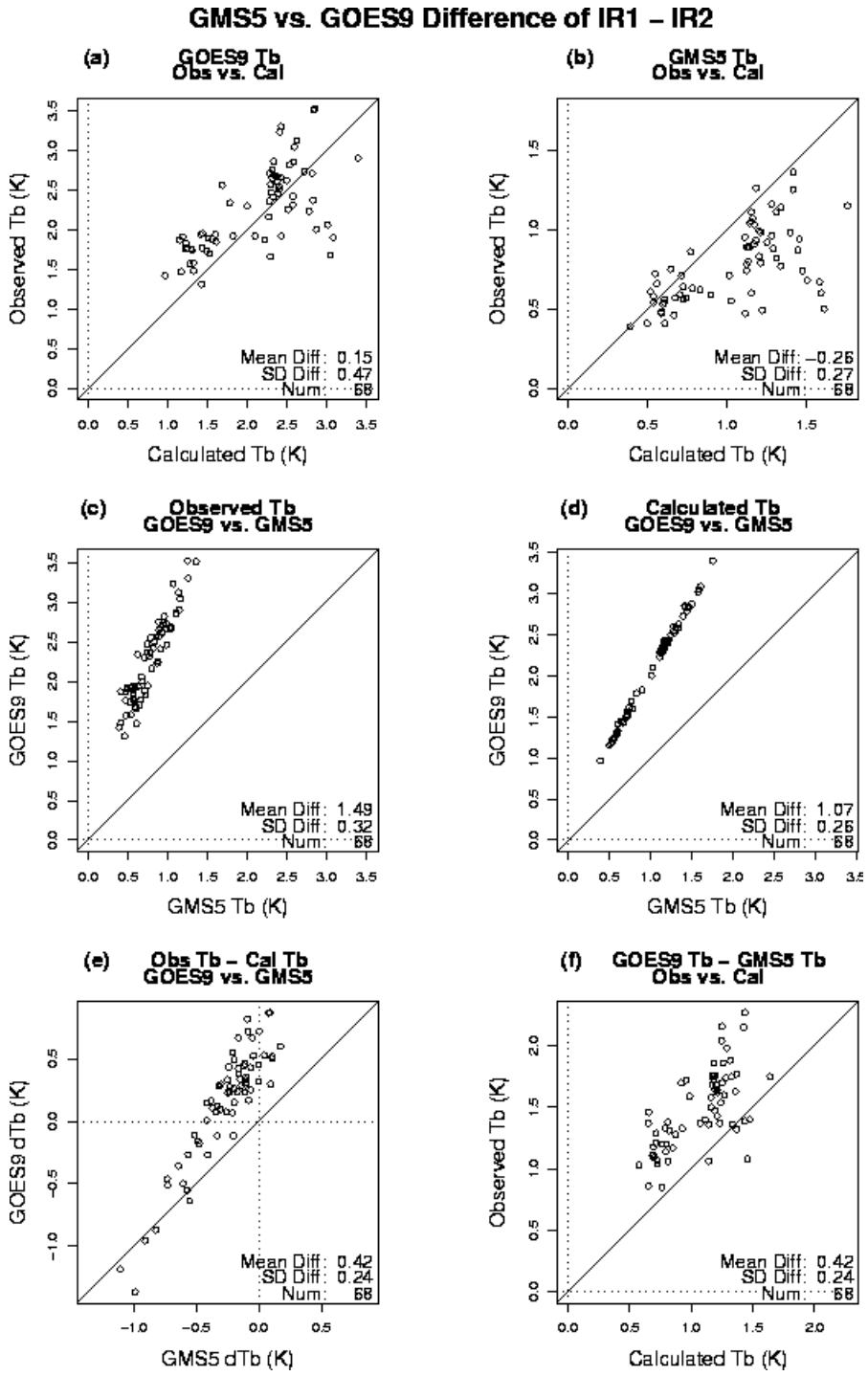

Figure 12: Same as Fig. 10, but the comparisons of differences in the brightness temperatures between the split window channels, $\delta T_{\mathrm{SP}} = T_{\mathrm{IR1}} - T_{\mathrm{IR2}}$.

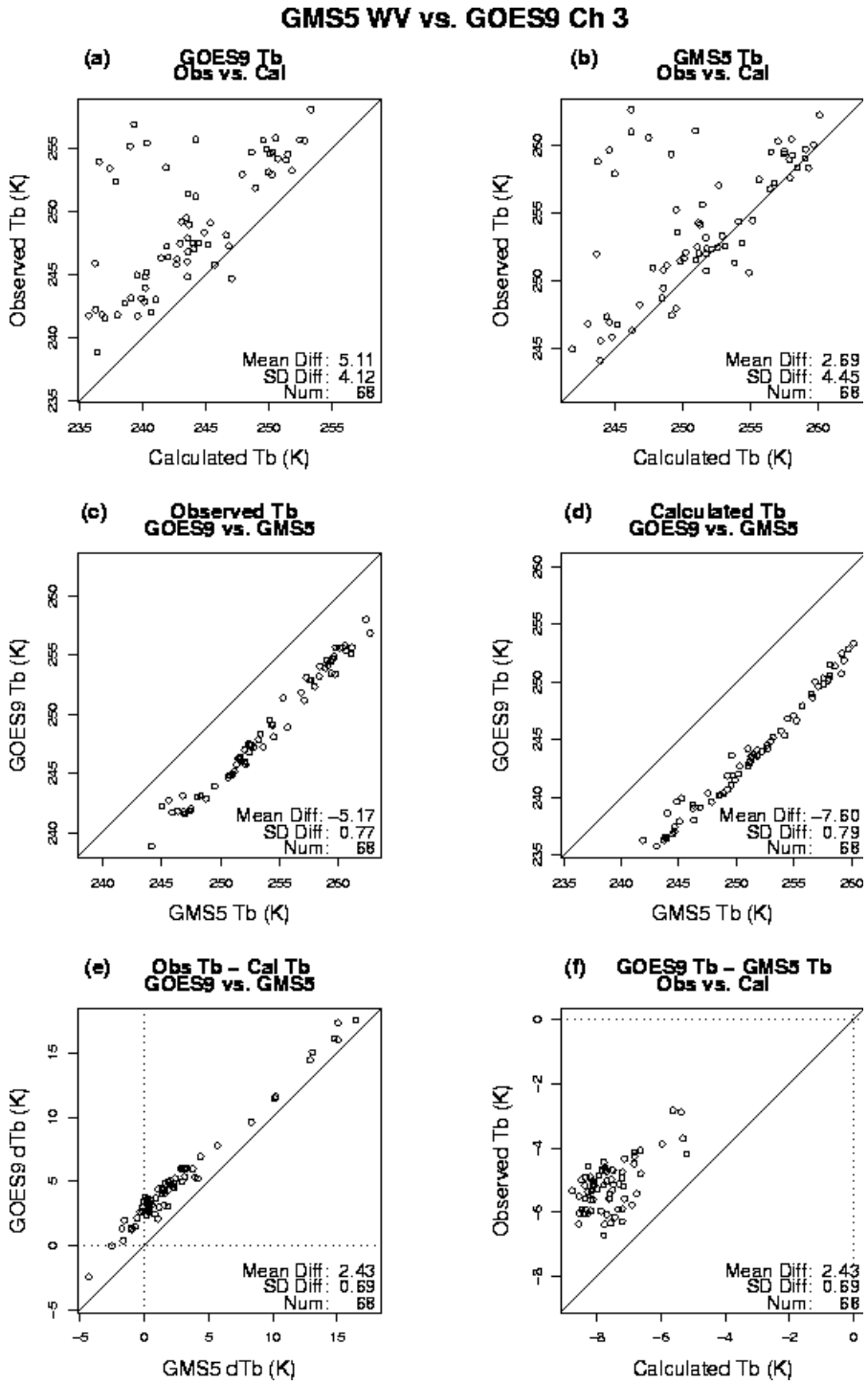

Figure 13: Same as Fig. 10, but the comparisons of WV brightness temperatures.